

A HIGH SWITCHING FREQUENCY IGBT PWM RECTIFIER/INVERTER SYSTEM FOR  
AC MOTOR DRIVES OPERATING FROM SINGLE PHASE SUPPLY

K. THIYAGARAJAH, V.T. RANGANATHAN and B.S. RAMAKRISHNA IYENGAR

Department of Electrical Engineering  
Indian Institute of Science  
Bangalore 560 012, INDIA

ABSTRACT

A PWM rectifier/inverter system using IGBTs, capable of switching at 20 kHz is reported. The base drive circuit for the IGBT, incorporating short circuit protection is presented. The inverter uses Undeland snubber together with a simple energy recovery circuit, which ensures reliable and efficient operation even for 20 kHz switching. The front end for the system is a regenerative single phase full-bridge IGBT inverter along with an AC reactor. The steady state design considerations are explained and control techniques, for unity power factor operation and fast current control of the front end converter, in rotating as well as stationary reference frames, are discussed and compared. Results from computer simulations as well as experimental results, for a 1.5 kW prototype system using GE type 6E20 IGBTs, are presented.

I. INTRODUCTION

High switching frequency inverters are desirable for A.C. motor drives, as they permit the operation of the drive with practically sinusoidal stator current and fast current control for high dynamic performance. In addition the audible noises can be reduced at switching frequencies of the order of 20 kHz.

Until recently, power bipolar transistors and MOSFETs have been commonly used for inverters driving A.C. motors. As a third possible alternative, Insulated-Gate-Bipolar-Transistors (IGBTs) have emerged recently. IGBTs offer low on resistance and require very little gate drive power. A 1.5 kw prototype PWM inverter using GE type 6E20 IGBTs is reported in this paper. A gate-drive circuit which provides fast turn-on and turn-off, and adequate protection against overload/shoot through faults is presented.

Switching aid networks (snubbers) are necessary to limit the stresses on the IGBTs at turn-on and turn-off. At high switching frequencies, the snubber losses become an appreciable portion of the output power, necessitating an energy recovery circuit to improve the efficiency. A simple and efficient energy recovery circuit which operates reliably at 20 kHz switching frequency is reported.

The front-end converter feeding a PWM inverter, should, ideally, regulate the D.C. link voltage, draw sinusoidal current from the A.C. mains, without drawing reactive power, and should have bidirectional power flow capability. A PWM type front-end converter with an A.C. reactor at the A.C. input side meets all the requirements and has been used as a voltage source for PWM inverters driving A.C. motors [1]. Control techniques for three-phase PWM type front-end converters have been reported [2,3,4]. There are applications, including single-phase A.C. traction, where operation from a single-phase supply is of interest and techniques of control in this context have been reported [5,6].

The A.C. motor drive system is shown in Fig. 1. The front-end for the system is a full-bridge IGBT PWM inverter with an A.C. reactor. The machine side converter is a high switching frequency IGBT three phase PWM inverter. The complete system operates from single-phase mains.

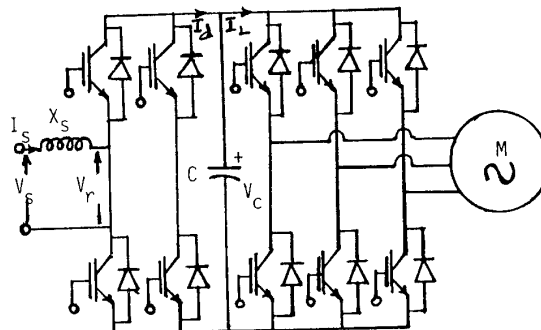


Fig. 1. IGBT PWM Rectifier/Inverter System

The steady state design considerations are explained and the block diagrams of control in rotating as well as stationary reference frame of the single-phase PWM type front-end converter are developed. The complexities of control implementation for the two control techniques are studied and compared in this paper.

II. 20 kHz IGBT INVERTER

II.1 Gate-Drive Circuit

The IGBT combines some of the features of both

bipolar-transistors and MOSFETs. It offers low saturation voltage and its voltage driven input, like that of a MOSFET, requires very little drive power. Its control terminals are the gate and emitter. The device turns-on when a voltage  $V_{GE}$  greater than gate-emitter threshold voltage  $V_{GEth}$  is applied between the gate and emitter. To turn-off the device a resistance  $R_{GE}$  must be connected between gate and emitter, which provides a discharge path for the gate-to-emitter capacitance. Unlike a MOSFET, the IGBT exhibits a long current fall time at turn-off. The fall time consists of two distinct intervals, one of which is constant and the other is a function of  $R_{GE}$ . The lower the value of  $R_{GE}$ , smaller is the turn-off time. However,  $R_{GE}$  has a minimum value below which the device may latch to the on state [7]. For fast turn-on of the IGBT, a sharp rising pulse of voltage level well above  $V_{GEth}$  is to be applied between gate and emitter. For fast turn-off the gate-to-emitter capacitance must be discharged quickly.

The gate-drive circuit developed for the IGBT is shown in Fig. 2. The speed-up capacitance  $C_p$  across  $R_{GS}$  provides a sharp rising edge while the device is turning-on. At turn-off the transistor  $Q_1$  turns-on temporarily and brings down the gate-drive pulse sharply. The gate-to-emitter capacitance discharges through the transistor  $Q_1$  and the device turns-off. The resistance  $R_{GE}$  improves the dV/dt capability of the IGBT.

The IGBT can latch to the on state if the maximum controllable current is exceeded. The gate-drive circuit must therefore provide protection against overload/shoot through faults. The protection against overload/shoot through faults is provided by sensing the collector-emitter

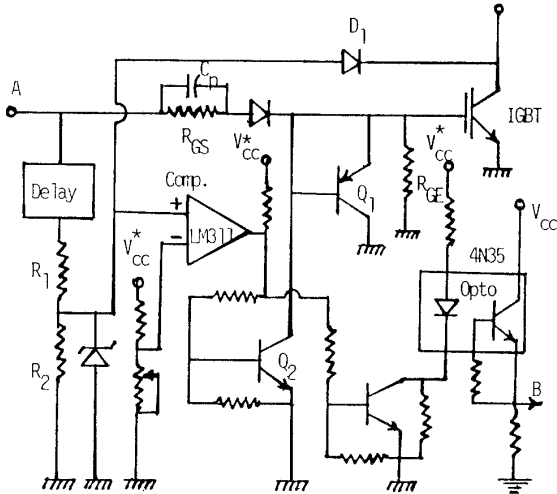


Fig. 2. Gate Drive Circuit for IGBT  
A - Isolated Gate Pulse; B - Trip Signal  
 $V_{cc}$  - Common Power Supply;  
 $V_{cc}^*$  - Isolated Power Supply

voltage through the diode  $D_1$ . In the gate-drive circuit of Fig. 2, the diode  $D_1$  is forward biased, during the normal operation of the device, and the output of the comparator remains low. In the event of a fault  $V_{CE}$  increases and  $D_1$  gets reverse biased. The output of the comparator goes high, if the potential at the positive input terminal (decided by  $R_1$ - $R_2$  network) is greater than the threshold set at the negative input terminal. The transistor  $Q_2$  turns-on and shuts off the gate-drive pulse. The device turns-off instantaneously. The opto-isolator gives out a trip-signal out of the isolated gate-drive circuit, which is used to diagnose the fault and take appropriate action in the controller. The protection is delayed to the extent of turn-on time of the device to avoid false tripping at turn-on.

## II.2 Snubber and Energy Recovery Circuit

To achieve reliable switching and to reduce the switching losses in the IGBTs switching aid networks are necessary for limiting dV/dt and di/dt. The Undeland snubber [8] is used as it has fewer components and introduces lower additional stresses to the switching devices and freewheeling diodes. In addition it confines the losses to one resistor making energy recovery simpler. The basic switching aid network is shown in Fig. 3. The prototype 1.5 kW inverter is designed to operate from a 220V D.C. bus, with a peak current of 20A. The corresponding snubber component values are shown in Fig. 3.

At the end of each switching the snubber energy is transferred to  $L_s$  and is dissipated in  $R_s$ . The energy dissipation in  $R_s$  causes an overvoltage on the device which turns off.

The turn-on energy loss is given by

$$W_{on} = (1/2) l_s \Delta I_{max}^2 \quad (1)$$

$$\text{where } \Delta I_{max}^2 = I_{rr}^2 + (C_s/l_s) V_{DC}^2 \quad (2)$$

$I_{rr}$  - Reverse recovery current of the freewheeling diode in Amps

$V_{DC}$  - D.C. bus voltage in volts.

The turn-off energy loss is given by

$$W_{off} = (1/2) l_s I_L^2 \quad (3)$$

where  $I_L$  - load current in Amps.

The snubber losses, for the component values shown in Fig. 3, approximately turn out to be 96W per leg at full load at 20 kHz switching frequency. The total power loss for the three-phase inverter, therefore becomes an appreciable portion (300W) of the output power. Hence an energy recovery circuit is used. The snubber with the energy recovery circuit is shown in Fig. 4. The features of the recovery circuit used are:

- i) Uses fewer components, than the self oscillating push-pull type described in [9]
- ii) Problem of flux resetting in the recovery transformer is eliminated

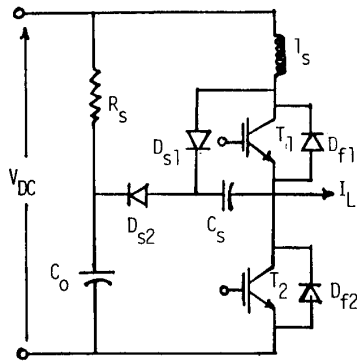


Fig. 3. Undeland Snubber Circuit  
 $l_s = 15 \text{ H}$ ;  $C_s = 0.1 \text{ F}$ ;  $C_o = 0.47 \text{ F}$

- iii) Operates reliably at 20 kHz switching frequency
- iv) Recovery takes place automatically after each switching, no additional control is required.

The operation of the recovery circuit is as follows. At the end of each switching the excess energy in the inductor  $l$  has to be discharged. To start with some of this energy is transferred to  $C_o$  and the voltage across  $C_o$  rises above the D.C. bus voltage  $V_{DC}$ . When the voltage rise is sufficient to turn-on the MOSFET through the  $R_1$ - $R_2$  network, the recovery transformer begins to conduct. The secondary winding  $N_s$  is clamped to the D.C. bus voltage  $V_{DC}$ , and therefore primary voltage gets clamped to  $(N_p/N_s)V_{DC}$ . This is also the voltage across  $l$  and therefore, the current in  $l$  drops at the rate of  $[(N_p/N_s)V_{DC}]/l$ . When the excess energy in the inductor is completely discharged the MOSFET turns-off automatically. Any residual energy in the core is returned to the D.C. bus through the tertiary winding  $N_R$ . The overvoltage across the devices, during the recovery process is given by

$$\Delta V_o = (N_p/N_s)V_{DC} \quad (4)$$

where  $N_p$  - number of turns on the primary

$N_s$  - number of turns on the secondary.

A turns ratio ( $N_p/N_s$ ) of 4 is used. Siemens pot-core type No. B85696-T26 is used for the transformer.

### II.3 Experimental Results

Figure 5 shows the experimental current waveforms of the recovery circuit. Referring to Fig. 5, it is seen that the recovery process is not so pronounced at turn-off. This is because the load current is much less compared to the value of the excess current  $\Delta I_{max}$  at the time of turn-on. The action of tertiary winding  $N_R$ , in resetting the transformer flux can also be clearly seen. From the device voltage waveforms in Fig. 6, it is seen that device voltage is not clamped tightly to the value expected  $(1 + N_p/N_s)V_{DC}$ . This is because of

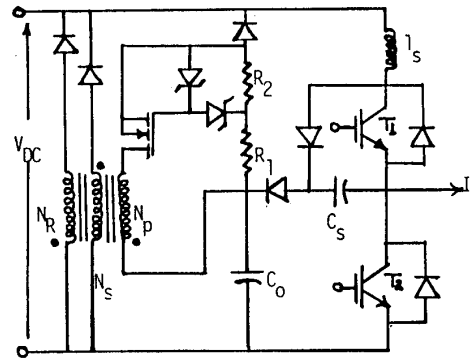


Fig. 4. Snubber with Recovery Circuit

the leakage inductance of the transformer. Also the capacitance  $C_o$  does not quite behave as a stiff voltage source. Therefore some additional oscillations are superimposed on the inductor current due to  $l_s - C_o$  resonance.

It can also be seen from the inductor current waveform, that the overshoot  $\Delta I_{max}$  at turn-on is less than the predicted value from Eq. (2). The reason is that the voltage across  $C_o$  tends to rise during the discharge of energy from  $C_s$ . This brings the recovery transformer into conduction and part of the energy in  $C_s$  is transferred to the



Fig. 5. Recovery Circuit Currents  
 a) Inductor, b) Primary, c) Secondary, d) Tertiary



Fig. 6 Device Voltage Waveforms  
 X: 10 sec/Divn. Y: 100V/Divn.

transformer leakage inductance. However, this energy along with the energy transferred to  $l_s$  is recovered through the recovery transformer. Measurement of the average values of the secondary and tertiary currents (using Yokogawa, Analysing Recorder model No. 3656) shows a total recovery of 54W under the test conditions.

### III. REGENERATIVE SINGLE-PHASE FRONT-END CONVERTER

#### III.1 Steady State Design Considerations

The single-phase front-end converter shown in Fig. 1 consists of a full-bridge inverter using IGBTs, with an A.C. reactor at the A.C. input side. The supply voltage  $V_s$  and the fundamental component  $V_r$  of the output voltage  $v_r(t)$  at the A.C. terminals of the inverter are two sinusoidal voltages separated by a reactor. The power flow therefore depends on the phase angle displacement between the two voltage phasors. The phasor diagram is shown in Fig. 7.

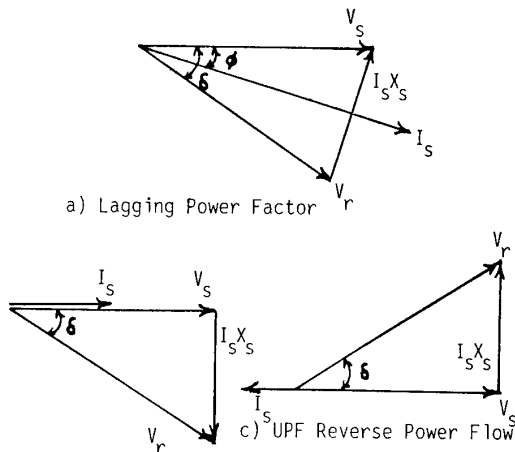


Fig. 7. Phasor Diagrams of the Front-end Converter

Power transferred from the source to the converter A.C. terminals is given by

$$P_{SR} = (V_s V_r / X_s) \sin \delta \quad (5)$$

$$= V_s I_s \cos \phi \quad (6)$$

where  $V_s$  - RMS value of the A.C. supply voltage (volts),

$V_r$  - RMS value of the fundamental component of the voltage generated at the A.C. terminal of the inverter (volts)

$\delta$  - Phase-angle displacement between voltage phasors  $V_s$  and  $V_r$

$X_s$  - Reactance<sup>s</sup> of the A.C. reactor at 50 Hz (ohm)

$\phi$  - Power-factor angle.

If the D.C. link voltage  $V_c$  is to remain constant then the input and output powers must be balanced.

From the phasor diagram of Fig. 7(a),

$$I_s \cos \phi = V_r \sin \delta / X_s \quad (7)$$

$$I_s \sin \phi = (V_s - V_r \cos \delta) / X_s \quad (8)$$

If the reactive power drawn from the mains is to be zero, then the power factor must be unity. Hence from equations (7) and (8)

$$I_s X_s = V_r \sin \delta \quad (9)$$

$$V_s = V_r \cos \delta \quad (10)$$

The phasor diagrams at unity power-factor operation for forward and reverse power flow are shown in Figs. 7(b) and 7(c), respectively. From equations (9) and (10)

$$V_r = \sqrt{V_s^2 + (I_s X_s)^2} \quad (11)$$

Under full-load conditions

$$V_{rFL} = V_s \sqrt{1 + X_{pu}^2} \quad (12)$$

$$\text{where } X_{pu} = (I_{sFL} X_s) / V_s \quad (13)$$

$I_{sFL}$  - full load RMS A.C. current assuming unity power-factor (Amps).

Equation (12) implies that  $V_r$  is greater than  $V_s$  by a factor  $\sqrt{1 + X_{pu}^2}$  known as the boost factor.

#### III.2 Design Considerations

The D.C. link voltage is decided by the line-to-line voltage rating of the motor. The D.C. link voltage together with the full-load power decides the voltage and current ratings of the power devices to be used. From the previous discussion the magnitude of  $V_r$  varies between a minimum of  $V_s$  to a maximum of  $V_s \sqrt{1 + X_{pu}^2}$ . This maximum value of  $V_r$  is decided by the maximum value of the phase separation which occurs under full load condition.

For a selected power device the minimum pulse or notch width that can be reliably reproduced in the inverter is decided by the device switching speeds and snubber relaxation times. The control technique adapted requires that the inverter always operate in full modulation; i.e. with modulation index ( $m$ ) less than or equal to one. The minimum value of  $m$  is decided by the fact that the minimum value of  $V_r$  is equal to  $V_s$

$$\text{i.e. } m_{\min} = V_s / (V_{DC} / \sqrt{2}) \quad (14)$$

It is desirable that, the reactor value is selected in such a way that, the maximum modulation index at which the inverter operates is as close to one as is permitted by the minimum pulse or notch width capability of the device. This is because under this condition the magnitude of  $V_r$  varies over a wide range making the control less sensitive to the errors in the controller gains, compensations, etc. If a very low value of inductance is used the range of variation of  $V_r$

becomes very much limited and the control becomes very sensitive to the above errors. Moreover the switching frequency has to be increased for a smaller reactor size in order to limit the current ripple. For a given minimum pulse or notch width the switching frequencies can only be increased upto the point where the minimum modulation index condition given by equation (14) is not violated.

Hence for a selected switching device the switching frequency should be selected so as to obtain a modulation index (m) close to one, under full load condition. With this maximum value of m, the corresponding values of  $V_{rFL}$  and hence  $X_{pu}$  can be calculated from equation (12). The size of C is decided by the amount of ripple voltage and current allowed at the D.C. link.

### III.3 Dynamic Control

The control philosophy is to regulate the D.C. link voltage, by matching the input power to the converter with the power demanded from the D.C. link, while maintaining the power-factor at unity for either direction of power flow. That is

$$V_s I_s = V_c I_d \quad (15)$$

$$\text{i.e. } (\sqrt{2} V_s \sqrt{2} I_s) / 2 = V_c I_d \quad (16)$$

$$\text{or } I_d = (\sqrt{2} V_s / 2 V_c) (\sqrt{2} I_s) \quad (17)$$

Therefore the amplitude of the A.C. input current must be controlled to balance the input and output powers of the converter, and it should be maintained in phase with  $V_s$ . The voltage regulation scheme can therefore be represented as shown in Fig. 8. The scheme consists of a fast inner current loop and an outer voltage loop.

The current loop of Fig. 8, can be realized by hysteresis current control of the PWM inverter [10]. However, the switching frequency is not constant in hysteresis control. Therefore the current harmonics injected into A.C. line are also not at fixed frequencies and cannot be filtered effectively. On the other hand, if the PWM inverter is operated as a voltage source inverter with sine-triangle modulation, the harmonics of the A.C. voltage and consequently the A.C. current occur at well defined frequencies. Therefore filters can be designed to suppress the A.C. current harmonics. In case of high power drives

the inverter can be split into several parts and harmonics can be cancelled out between part inverters by phase shifting the carrier waveforms [11]. This realization has led to the investigation of voltage source operation for the front-end converter with sine-triangle modulation [2,12]. In general, current control of voltage source inverters can be accomplished either in rotating or stationary reference frame [13]. For inverters driving A.C. motors at variable frequency, the phase errors introduced by stationary reference frame control are difficult to compensate and so rotating reference frame control is preferred. For inverters operating from fixed frequency three-phase mains, there is no significant difference in the complexity of implementation between the two techniques [4]. However, control in stationary coordinates with correction for the phase-lag produced by the control loop seems to have been favoured [2,4].

The present work is focused on single-phase systems. This is because for low power drives, the input is more likely to be single phase. Many UPS systems also operate from single phase supply and a single-phase front-end converter can be used [14]. Another important application for single-phase system is that of A.C. traction.

In the following the current control of the single-phase voltage source PWM inverter is studied in rotating as well as stationary reference frames. The block diagrams of the control system are developed.

### III.4 Control in Rotating (d-q) Reference Frame

The usual advantage sited for the use of rotating reference frame control is that the control loops work on D.C. quantities and the bandwidth requirements on the controllers are less demanding. However, all feedback quantities have to be translated into the rotating reference frame. In the present case, this implies isolating the direct (or active) component  $i_{sq}(t)$  and the quadrature (or reactive) component  $i_{sq}(t)$  of the A.C. current  $i_s(t)$ . The modelling of the system, for the d-q reference frame of control is carried out as follows. The instantaneous values of supply voltage  $v_s$ , supply current  $i_s$  and the converter A.C. terminal voltage  $v_r$  can be expressed as follows

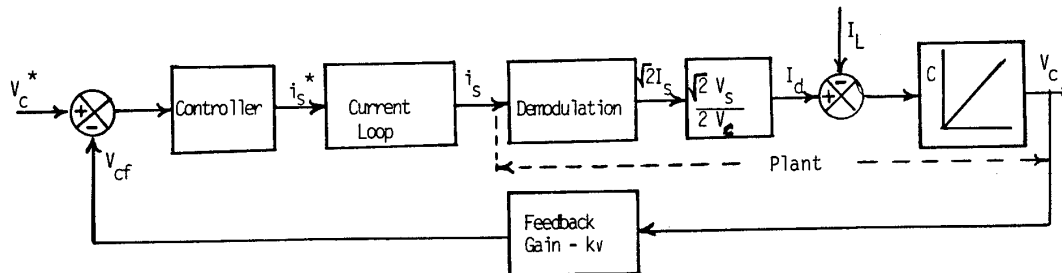


Fig. 8. Block Diagram for D.C. Voltage Regulation

$$v_s(t) = \sqrt{2} V_s(t) \sin \omega t \quad (18)$$

$$i_s(t) = i_{sd}(t) \sin \omega t + i_{sq}(t) \cos \omega t \quad (19)$$

$$v_r(t) = v_{rd}(t) \sin \omega t + v_{rq}(t) \cos \omega t \quad (20)$$

where the subscript 'd' denotes the quantities in phase with  $V_s$  and 'q' denotes the quantities in quadrature with  $V_s$ .

The voltage equation for the single phase system is given by

$$v_s(t) = L_s \frac{di_s(t)}{dt} + v_r(t) \quad (21)$$

Substituting equations (18), (19) and (20) into equation (21) and collecting  $\sin \omega t$  and  $\cos \omega t$  terms separately the following equations for the currents can be obtained.

$$L_s \frac{di_{sd}(t)}{dt} = \sqrt{2} V_s(t) + \omega_s L_s i_{sq}(t) - v_{rd}(t) \quad (22)$$

$$L_s \frac{di_{sq}(t)}{dt} = -\omega_s L_s i_{sd}(t) - v_{rd}(t) \quad (23)$$

Considering the equation (22), the plant for current loop can be represented as shown in Fig. 9 for the d-axis. A similar diagram can be drawn for the q-axis, by considering equation (23).

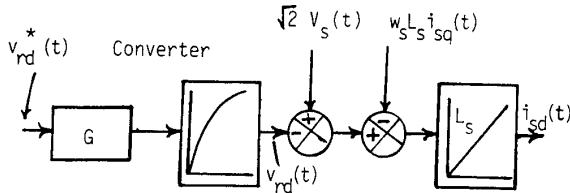


Fig. 9. Control Plant for d-axis Current Loop

If the desired response of the current loop is a first order lag of  $T$ , then the dynamics of the current loops can be described by the following equations.

$$T \frac{di_{sd}(t)}{dt} + i_{sd}(t) = \frac{i_{sd}^*(t)}{K_i} \quad (24)$$

$$T \frac{di_{sq}(t)}{dt} + i_{sq}(t) = \frac{i_{sq}^*(t)}{K_i} \quad (25)$$

where  $T$  - lag of the converter corresponding to the switching frequency

$K_i$  - current feedback gain  
superscript \* denotes the control signals for the reference values.

Comparing equations (22) and (24) the control law for  $v_{rd}^*(t)$  can be written as

$$v_{rd}^*(t) = \frac{\sqrt{2} V_s(t)}{G} + \frac{\omega_s L_s (K_i i_{sq}^*(t))}{G K_i} - \frac{L_s}{T} \frac{1}{G K_i} [i_{sd}^*(t) - K_i i_{sd}(t)] \quad (26)$$

Similarly comparing equations (23) and (25) the control law for  $v_{rq}^*(t)$  is written as

$$v_{rq}^*(t) = \frac{-\omega_s L_s (K_i i_{sd}(t))}{G K_i} - \frac{L_s}{T} \frac{1}{G K_i} [i_{sq}^*(t) - K_i i_{sq}(t)] \quad (27)$$

The block diagram of the control scheme for the d-axis according to equations (22) and (26) is shown in Fig. 10. An outer voltage control loop is provided to regulate the D.C. link voltage. The instantaneous value of the D.C. link voltage is compared with a reference, and the error after passing through a controller, is used as the reference signal for the d-axis current. The feed-forward load compensation is used, so that the system can be stabilized with a simple P-controller for the voltage control loop. The gain of the P-controller is calculated, following the usual linear control system theory.

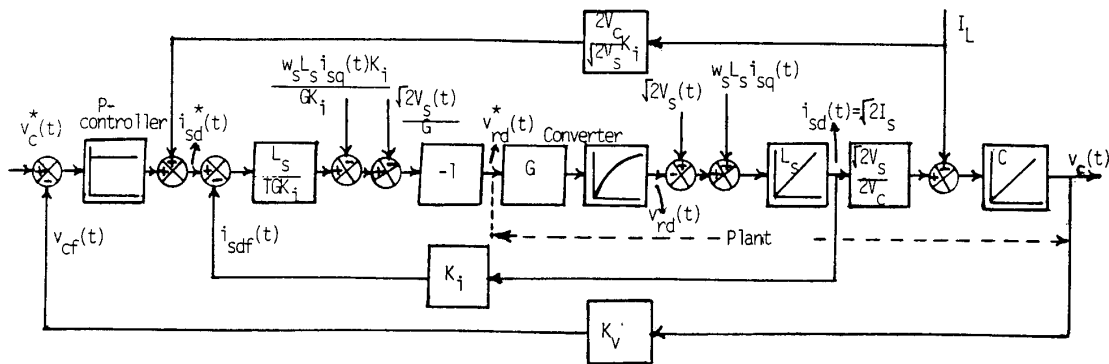


Fig. 10. Block Diagram of Voltage Regulation Scheme Showing Current Loop in d-axis

The control scheme for the q-axis is similar except that the reference for q-axis current is fixed at zero, since for unity power factor operation the q-axis current must be forced to zero.

As seen from the block diagram of Fig. 10, the control scheme requires the d and q-axis components of the A.C. current as feedback signals. These components of the current are calculated as follows.

Multiplying equation (19) by  $\sin \omega t$

$$i_s(t) \sin \omega t = i_{sd}(t) \sin^2 \omega t + i_{sq}(t) \cos \omega t \sin \omega t$$

$$= \frac{i_{sd}(t)}{2} - \frac{i_{sd}(t)}{2} \cos 2\omega t + \frac{i_{sq}(t)}{2} \sin 2\omega t \quad (28)$$

Multiplying equation (19) by  $\cos \omega t$

$$i_s(t) \cos \omega t = i_{sd}(t) \sin \omega t \cos \omega t + i_{sq}(t) \cos^2 \omega t$$

$$= \frac{i_{sd}(t)}{2} \sin 2\omega t + \frac{i_{sq}(t)}{2} + \frac{i_{sq}(t)}{2} \cos 2\omega t \quad (29)$$

If the double frequency components present in equations (28) and (29) are filtered, then  $i_{sd}(t)$  and  $i_{sq}(t)$  can be obtained. The calculation of  $i_{sd}(t)$  and  $i_{sq}(t)$  is shown in the block diagram of Fig. 11.

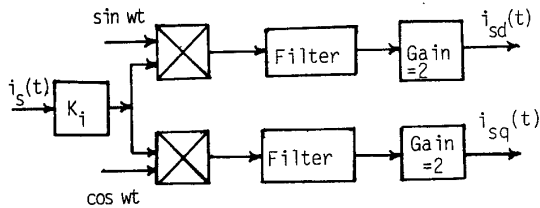


Fig. 11. Block Diagram for Calculation of  $i_{sd}$  &  $i_{sq}$

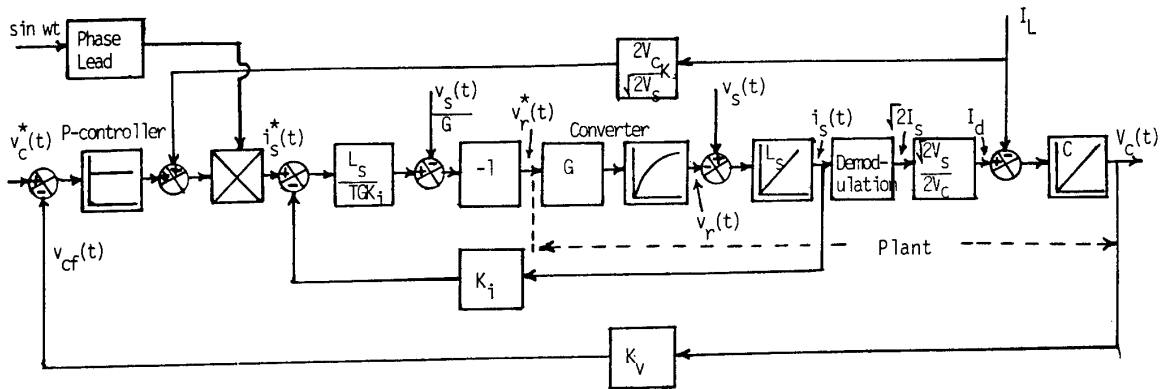


Fig. 13. Block Diagram of Voltage Regulation Scheme with Current Control in Stationary Coordinates

To eliminate the double frequency components, it would appear that a simple low pass filter would be sufficient. But the desired closed loop response as assumed in Eqs. (24) and (25) corresponds to a closed loop bandwidth of about 160 Hz. Therefore the introduction of low pass filters to eliminate the double frequency component will adversely affect the response of the current loops. It was found through computer simulation that only a notch filter designed to eliminate the double frequency components gave satisfactory results.

### III.5 Control in Stationary Reference Frame

In stationary reference frame of control the inner current loop will be working with A.C. quantities, while the outer voltage control loop will be working with D.C. quantities. The modelling of the system is carried out as follows. The voltage equation (21) can be rewritten as

$$L_s \frac{di_s(t)}{dt} = v_s(t) - v_r(t) \quad (30)$$

According to equation (30) the plant for current loop can be represented as shown in Fig. 12.

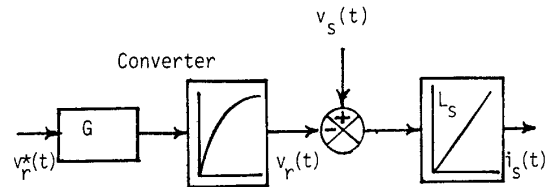


Fig. 12. Control Plant for Current Control in Stationary Coordinates

As before if the desired response of the current loop is a first order lag of  $T$ , then the dynamics of the current loop can be described by the following equation:

$$T \frac{di_s(t)}{dt} + i_s(t) = \frac{i_s^*(t)}{K_i} \quad (31)$$

The reference  $i_s^*(t)$  is sinusoidal and hence the response  $i_s(t)$  will also be sinusoidal with a phase lag of  $\arctan \omega T$ . This phase lag can be compensated by introducing a corresponding phase lead for the current reference  $i_s^*(t)$ . Comparing equations (30) and (31) the control law for  $v_r^*(t)$  is written as

$$v_r^*(t) = \frac{v_s(t)}{G} - \frac{L}{T} \frac{1}{GK_i} [i_s^*(t) - K_i i_s(t)] \quad (32)$$

The block diagram of control scheme, in stationary reference frame, according to equations (30) and (32) is shown in Fig. 13. This scheme also consists of an outer voltage control loop with a P-controller and feed-forward compensation for the load current. The current reference is given a phase lead, to account for the phase lag introduced by the loop. The gain of P-controller is calculated following the usual linear control system theory.

### III.6 Computer Simulation

The simulation results of the front-end converter are obtained using the simulation software TUTSIM [15]. The switching process of the front-end converter with sine-triangle modulation is represented in the simulation. Figs. 14 and 15 show the simulated results for the rotating reference frame control and the stationary reference frame control respectively. The results show that there are no significant differences between the two techniques of control described above, as far as the performance of the converter is concerned. Hence considering the difficulties in obtaining the d and q-axis components of A.C. current as feedback signals in rotating reference frame control, the stationary reference frame control is easier to implement. The phase error introduced by the control loop can be easily compensated as the front-end converter operates from a fixed frequency A.C. voltage source.

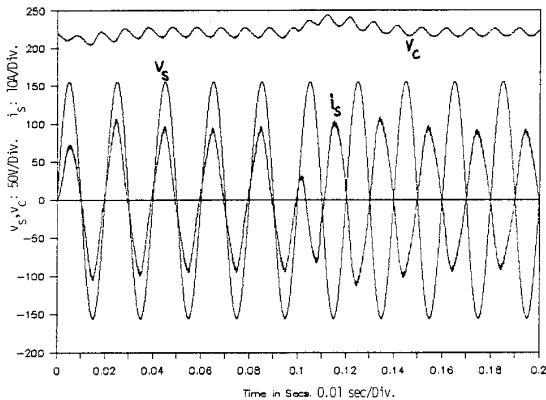


Fig.14. Simulated Waveforms for d-q Reference Frame Control. Step Reversal of Load at 0.1 sec.

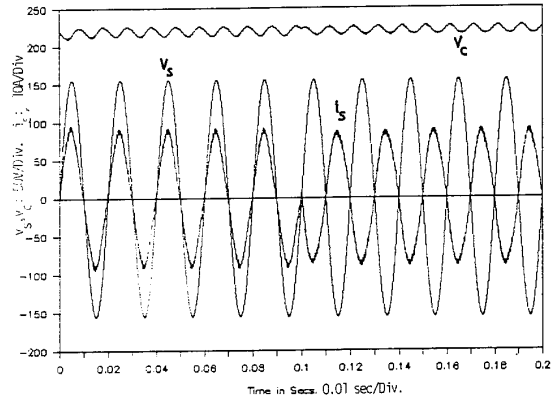


Fig.15. Simulated Waveforms for Stationary Reference Frame Control. Step Reversal of Load at 0.1 sec.

### III.7 Experimental Results

A prototype 1.5 kW laboratory model of the front-end converter is made using GE Type IGBT 6E20. The A.C. current is sensed by a simple inexpensive current sensor. The D.C. load current, for feed-forward compensation, is sensed by Hall-effect current transducer. The reference sine wave is obtained through a potential transformer connected across the A.C. supply terminals. The control scheme is as shown in Fig. 13. The converter is operated with sine-triangle modulation with a carrier frequency of 1 kHz. The gains in the controller are adjusted for nominal A.C. supply voltage of 110V (rms) and D.C. link voltage of 220V and the proportional gain is adjusted to 5.

To start with, the D.C. link capacitor is charged through the diodes of the front-end converter itself with the gating pulses to IGBTs being blocked. When the gate pulses are released, the D.C. link voltage builds up to the reference value set by the voltage control loop.

Figure 16 shows the experimental waveforms of AC supply voltage and current at 45% of full load for forward power flow. It is seen that A.C. current is near sinusoidal at unity power factor.

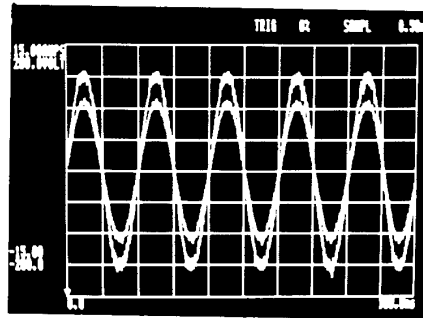


Fig. 16. A.C. Voltage and Current - Forward Power Flow. X: 10 msec/Div.,  $Y_1$ : 50V/Div.,  $Y_2$ : 3.75A/Div.



## REFERENCES

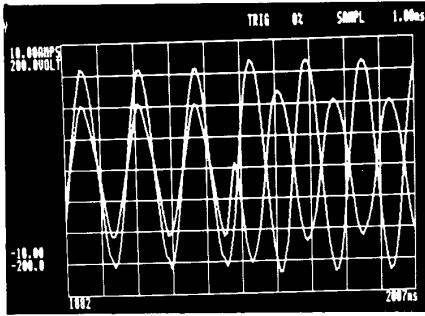


Fig.17.A.C.Voltage and Current for Step Reversal of Power Flow.X:12.5 msec/div.  $Y_1$ :50V/Div.  $Y_2$ :2.5A/Div

Figures 17 shows the transient waveforms for a step change of load current from one direction to the other. The system responds as expected, and has a high dynamic performance. Fig. 18 shows that there is practically no change in the D.C. link voltage even when the load current changes from one direction to the other, in step fashion.

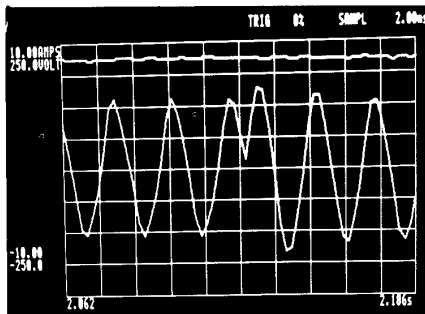


Fig. 18. D.C.Link Voltage and A.C. Current for Step Reversal of Power Flow.  
X: 12.5 msec/Div.,  $Y_1$ :62.5V/Div.,  $Y_2$ : 2.5A/Div.

## IV. CONCLUSION

An inverter/converter system operating from a single-phase supply has been described. The power device used in the system is the IGBT. The inverter can operate at switching frequencies upto 20 kHz. Snubber circuits along with energy recovery networks suitable for such high frequency of operation have been described and experimental results from a laboratory inverter have been presented.

The steady-state design considerations of the front-end converter have been discussed. The block diagrams for dynamic control in rotating as well as stationary reference frames have been developed. Experimental results from a laboratory converter with stationary reference frame control have been presented in support of the analysis.

1. Helmut Kohlmeier, Olaf Niermeyer, and Dierk F. Schroder, 'Highly Dynamic Four-quadrant A.C. Motor Drive with Improved Power Factor and On-line Optimised Pulse Pattern with PROMC', IEEE Trans. IAS, Vol. IA-23, No. 6, pp. 1001-1009, Nov/Dec. 1987.
2. Rusong Wu, S.B. Dewan, G.R. Slemon, 'A PWM AC to DC Converter with Fixed Switching Frequency', IEEE IAS Annu. Meeting, pp. 706-711, 1988.
3. J.W. Dixon, B.T. Ooi, 'Dynamically Stabilized Indirect Current Controlled SPWM Boost Type-3 Phase Rectifier', IEEE IAS Annu. Meeting, pp. 702-705, 1988.
4. Hidehiko Sugimoto, Siegeo Morimoto and Masoo Yano, 'A High Performance Control Method of a Voltage Type PWM Converter', IEEE PESC Record, pp. 360-368, 1988.
5. G. Klinger, 'Regelungstechnische Untersuchung Einer Einphasenstromrichterschaltung Mit Harmonische Zeitvariantem Ubertrager', Proceedings IFAC Symposium in Control in Power Electronics and Electrical Drives, Vol. 1, pp. 443-456, Dusseldorf, 1974.
6. Omar Stihi, B.T. Ooi, 'A Single Phase Controlled-Current PWM Rectifier', IEEE Trans. on Power Electronics, Vol. 3, No. 4, pp. 453-459, 1988.
7. B.J. Baliga and Marvin Smith, General Electric Co., 'Modulated-Conductivity Devices Reduce Switching Losses', EDN, pp. 153-162, Sept. 29, 1983.
8. T. Undeland, F. Jensen, A. Steinbakk, T. Rogne, M. Hernes, 'A Snubber Configuration for Both Power Transistor and GTO PWM Inverters', IEEE PESC Record, pp. 42-53, 1984.
9. Johan C. Bendien, Heinz Van Der Broeck, Gert Fregien, 'Recovery Circuit for Snubber Energy in Power Electronic Applications with High Switching Frequencies', IEEE Trans. on Power Electronics, Vol. 3, No. 1, pp. 26-30, 1988.
10. J.W. Dixon, A.B. Kulkarni, M. Nishimoto, B.T. Ooi, 'Characteristics of a Controlled Current PWM Rectifier-Inverter Link', IEEE IAS Annu. Meeting, pp. 685-691, 1986.
11. A. Schonung, H. Stemmler, 'Static Frequency Changers with Subharmonic Control in Conjunction with Reversible Variable-Speed A.C. Drives', The Brown Boveri Review, Vol. 51, No. 8/9, pp. 555-577, Aug/Sept. 1964.
12. J.W. Dixon, B.T. Ooi, 'Indirect Current Control of a Unity Power Factor Sinusoidal Current Boost Type Three-Phase Rectifier', IEEE Trans. on Industrial Electronics, Vol. 35, No. 4, pp. 508-515, Nov. 1988.
13. Colin, D. Schauder, Roy Caddy, 'Current Control of Voltage-Source Inverters for Fast Four-Quadrant Drive Performance', IEEE Trans. IAS, Vol. IA-18, No. 2, pp. 163-171, Mar/Apr. 1982.
14. Takami Kagotani, Kazuo Kuroki, Junichi Shinohara, Akira Misalzu, 'A Novel UPS Using High-Frequency Switch-Mode Rectifier and High Frequency PWM Inverter', IEEE PESC Record, pp. 53-57, 1989.
15. TUTSIM - TUTSIM User's Manual, TUTSIM Products, 200, California Avenue, # 212, Palo Alto, California, 94306, USA.